Design of Artificial-Materials-based Antennas Using Inverse Scattering Techniques

R. Palmeri, M. T. Bevacqua, A. F. Morabito, and T. Isernia

***Abstract*— A new approach to the design of Graded Artificial Material (GAM)-based devices is proposed by exploiting the inverse scattering framework as a synthesis tool. The introduced general methodology can be applied to arbitrary far-field specifications, thus allowing the design of non-canonical devices. In particular, two different strategies are developed for GAMs based on either graded refractive index (GAM_R) or graded filling factor (GAM_F). In both strategies, the inverse scattering problem is solved by a proper reformulation of the Contrast Source Inversion method, wherein a proper rescaling of the amplitude of the primary sources is also used. In particular, in the first strategy, the GAM_F is obtained by exploiting homogenization theories. In the second strategy, the GAM_R is synthesized by exploiting a suitable representation basis for the unknown contrast function, and, then, simple analytical formulas are used to determine the corresponding GAM_F. The proposed approach is assessed through the synthesis of an antenna generating a Σ/Δ reconfigurable pattern.**

***Index Terms*—Antenna synthesis, flat antennas, gradient index lens, homogenization, inverse scattering, reconfigurable patterns.**

I. Introduction

GRADED Refractive INdex (GRIN) media enable the control of the electromagnetic field paths. Classical GRIN devices are the Luneburg lens [1],[2] and the Maxwell fish-eye lens [3] (with their variants [4]–[8]). These elegant analytical solutions of the Maxwell equations allow for the design and building of useful antennas and devices; however, they just represent a very restricted set of the different electromagnetic field behaviors that one can pursue using a GRIN-based antenna.

To enforce a different given behavior of the electromagnetic field, some general framework and suitable techniques are required.

As one possibility, Transformation Optics (TO) theory [9] provides a general methodology for controlling the electromagnetic waves propagation by tailoring the spatial constitutive profile of a material [4]-[7],[10],[11]. Unfortunately, the bi-anisotropic materials generally obtained by TO are so complicated that they cannot be easily realized. Thus, to more easily manufacture electromagnetic devices, one can relax the exact required parameters of the material at the cost of an unavoidable deterioration of the performances.

A suitable and more flexible alternative method, introduced in [12] and recently re-proposed by the present research group [13]-[15], is based on inverse scattering theory, which provides an interesting framework for the synthesis of dielectric profile antennas and other devices. In fact, this method represents a general methodology that allows control of the electromagnetic waves path to obtain arbitrary field specifications.

Inverse scattering techniques [16],[17] are currently widely exploited for non-invasive microwave imaging and diagnostics. Indeed, in an inverse scattering problem (ISP), the aim is to retrieve the location, shape and electromagnetic properties of an unknown object starting from the knowledge of the incident field and the measurements of the arising scattered or total field. Such diagnosis problem can be transformed into a synthesis problem by considering a specific behavior of the total field as available data of the problem (rather than the measured total field). In this case, the new aim of the problem is to determine the dielectric profile of an object such that the interaction with an impinging wave will give rise to the specified total field.

Notably, the solution of an ISP represents a very difficult task as it is non-linear and can give rise to the so-called “false solutions” [18], which could be completely different from the actual ground truth. However, in the adoption of inverse scattering techniques as a design tool, the non-linearity of the ISP is not equally problematic. In fact, any dielectric profile is admissible as long as a good matching with the expected field characteristics is achieved.

From a practical perspective, the realization of a GRIN lens with a generic gradient index profile poses difficult fabrication challenges. Hence, investigations have been performed on stepped-index lenses [19]–[21], in which the desired continuous variation of the refraction index with radius is approximated by a number of constant-index spherical shells. As it can be expected, such a strategy results in a tradeoff between the number of shells and the achieved performances.

Recently, more effective fabrication techniques have been developed based on the use of Graded Artificial Materials (GAMs) [22]–[26], through which the guiding of the electromagnetic waves is performed using a well-designed spatially dependent dispersion, i.e., by engineering the filling

This is the post-print of the following article: R. Palmeri, M. T. Bevacqua, A. F. Morabito, and T. Isernia, “Design of Artificial-Material-Based Antennas Using Inverse Scattering Techniques,” IEEE Transactions on Antennas and Propagation, vol. 66, n. 12, pp. 7076-7090, 2018. Article has been published in final form at: https://ieeexplore.ieee.org/document/8470142. DOI: 10.1109/TAP.2018.2871707.

factor, the lattice period, and/or the material index of the device. Such structures are widely used in the literature, and good results have been obtained for the realization of canonical lenses [8], [27]–[31]. The design of the above-described GAMs-based canonical lenses is essentially based on the homogenization theory, with the Maxwell-Garnett effective medium [32] being the most frequently used technique. To the best of our knowledge, there is no general approach in the literature to synthesize Artificial Materials (AM) based devices for the case of (non-canonical) lenses realizing an arbitrarily given electromagnetic field behavior.

In this paper, we introduce a general methodology that can be applied to arbitrary field specifications and allows the design of two-dimensional GAMs by exploiting the inverse scattering framework. It is important to underline that, different from approaches [12]-[15], in the proposed approach multi-purpose devices are dealt with and the practical realization issue is addressed by taking advantage from AM. In particular, the design of an AM-based lens antenna is pursued. Besides being a step toward the realization of 3D antennas, consideration of 2D AM-based devices has an interest *by per se*. In fact, a practical implementation can be considered by using parallel plate waveguides [33]–[34], such that a proper 'arraying' along the residual direction can allow actual 3D design solutions. Moreover, the 2D problem herein considered shows an interesting relationship with the synthesis of flat antennas, whose interest is recently growing [35]–[38]. In fact, in both cases, one must realize a proper arrangement of the field paths along a plane.

The overall procedure consists of two steps. In the first step, a far-field pattern obeying some mask constraints is synthesized. In the second step, the ISP is solved to synthesize a device able to radiate the far-field pattern resulting from the previous step. Because the final goal of the approach is to design a GAMs device with a gradient of the filling factor, we propose and compare two different strategies to accomplish such a goal. In particular, a first and more intuitive possibility concerns the use of the effective medium theory on the obtained continuous GRIN profile. As a second and more original possibility, we propose an approach based on the use of a convenient basis expansion of the unknown contrast function and simple analytical arguments.

The paper is structured as follows. In Section II, the basics of the ISP and the Contrast Source Inversion (CSI) [39]–[41] method are reviewed. In Section III, a novel reformulation of the CSI is given, allowing for tuning of the amplitude of the primary sources. The two GAMs synthesis procedures are explained in Section IV. Finally, in Section V, the proposed approach is assessed through the design of an antenna for radar applications. The conclusions are presented last.

II. The Inverse Scattering Problem and the Contrast Source Inversion Method

Let us consider a region of interest Ω in which the background medium is air ($\varepsilon_b = 1$, $\sigma_b = 0$ being the relative permittivity and conductivity, respectively), and let Γ_t and Γ_o be the illumination and the observation surface, respectively.

For a 2D TM scalar problem (and by omitting the implicit time harmonic factor $\exp(j\omega t)$), a rather usual formulation of the ISP [16],[17] reads:

$$E_s(\boldsymbol{r_o}, \boldsymbol{r_t}) = \mathcal{A}_e[W(\boldsymbol{r}, \boldsymbol{r_t})] = -\frac{j\beta_0^2}{4}\int_\Omega H_0^{(2)}(\beta_0|\boldsymbol{r_o} - \boldsymbol{r}'|)W(\boldsymbol{r}', \boldsymbol{r_t})d\boldsymbol{r}', \quad \boldsymbol{r} \in \Omega \tag{1}$$

$$W(\boldsymbol{r}, \boldsymbol{r_t}) - \chi(\boldsymbol{r})E_i(\boldsymbol{r}, \boldsymbol{r_t}) = \chi(\boldsymbol{r})\mathcal{A}_i[W(\boldsymbol{r}, \boldsymbol{r_t})] = -\frac{j\beta_0^2}{4}\chi(\boldsymbol{r})\int_\Omega H_0^{(2)}(\beta_0|\boldsymbol{r} - \boldsymbol{r}'|)W(\boldsymbol{r}', \boldsymbol{r_t})d\boldsymbol{r}', \quad \boldsymbol{r} \in \Omega \tag{2}$$

where E_i and E_s are the incident and scattered field, respectively, $W = \chi E_t$ is the so-called contrast source, and $E_t = E_i + E_s$ is the total field. The kernel $H_0^{(2)}(\beta_0 \boldsymbol{r})$ of the integral operator is the Hankel function of zero order and second kind, β_0 is the wavenumber in the background medium, $\boldsymbol{r_t} = (r_t, \theta_t)$ and $\boldsymbol{r_o} = (r_o, \theta_o)$ are the illumination and the observation positions, respectively, while $\mathcal{A}_e$ and $\mathcal{A}_i$ are a short notation for the integral radiation operators.

ISP aims at retrieving the contrast function χ starting from the knowledge of the scattered field E_s on Γ_o. The contrast function $\chi(\boldsymbol{r}) = (\tilde{\varepsilon}_r(\boldsymbol{r}) - \varepsilon_b)/\varepsilon_b$ encodes the electromagnetic properties of the region Ω; in particular, $\tilde{\varepsilon}_r(\boldsymbol{r}) = \varepsilon_r(\boldsymbol{r}) - j\sigma_r(\boldsymbol{r})/\omega\varepsilon_0$ is the complex relative permittivity, ω being the angular frequency and ε_0 the permittivity of the vacuum.

As it is well known, ISP is non-linear since both the contrast function χ and the contrast source W are unknowns [16],[17]. In order to face such a difficulty, several efforts have been carried out in the literature to develop effective solution methods [18],[39]–[43]. The CSI method [39],[40] is one of the most popular and effective inversion schemes. As a matter of fact, it allows to face ISP in its full non-linearity, while dealing with a mathematical problem involving just linear and quadratic equations.

In particular, it simultaneously looks for both the contrast χ and the contrast source W, and the solution is iteratively built by minimizing the cost functional (3), which takes into account the data-to-unknown relationship and the physical model [18],[39]–[41]:

$$\phi(W, \chi) = \sum_{v=1}^{T}\frac{\left\|\mathcal{A}_e[W^{(v)}] - E_s^{(v)}\right\|_2^2}{\left\|E_s^{(v)}\right\|_2^2} + \sum_{v=1}^{T}\frac{\left\|\chi\mathcal{A}_i[W^{(v)}] + \chi E_i^{(v)} - W^{(v)}\right\|_2^2}{\left\|\chi E_i^{(v)}\right\|_2^2} \tag{3}$$

where the dependence on $\boldsymbol{r}$ and $\boldsymbol{r_o}$ has been omitted for the sake of brevity, while the dependence from $\boldsymbol{r_t}$ is identified by the superscript v. $\|\cdot\|_2$ is the ℓ_2-norm and T is the number of different incident fields corresponding to different positions $\boldsymbol{r_t}$.

As proposed in [41], the minimization of (3) can be pursued by means of a conjugate gradient algorithm in which, at each step, the values of χ and $W^{(v)}$ are updated by a line

minimization procedure. Obviously, other minimization schemes (including off the shelf numerical routines) can be used. In fact, this will not affect the final results, the only resulting difference being the computational time.

III. A MODIFIED CSI AS A DESIGN TOOL

When a synthesis problem is considered instead of a diagnostic one, the aim becomes determining $\chi(\boldsymbol{r})$ starting from the knowledge of the incident field and obeying given specifications of the total field. Let us note explicitly that design constraints are given in terms of the total fields; this approach is slightly different from the typical ISP, where equations are usually written in terms of the scattered field. Obviously, one can easily go from one formulation to another by simply subtracting or adding the incident fields.

Note that for a given total field on the observation domain Γ_o, different amplitudes of the incident fields give rise to different requirements on the scattered fields (and hence to different profiles). For this reason, differently from approaches [12]-[15], it proves convenient to modify the standard CSI algorithm by considering one more set of complex unknowns $\tau^{(v)}$ modulating the amplitudes of the primary sources. In fact, exploitation of these additional degrees of freedom will allow for a better matching of the desired fields and/or to simpler contrast profiles. Thus, it is convenient to distinguish among a 'basic' incident field $\hat{E}_i^{(v)}$(corresponding to unitary excitation) and an 'actual' incident field E_i (corresponding to the synthesized excitations of the primary sources times of the relevant $\hat{E}_i^{(v)}$).

Accordingly, the CSI functional is recast as follows:

$$\phi(W,\chi,\tau) = \sum_{v=1}^{T} \frac{\left\| \mathcal{A}_e\left[W^{(v)}\right] - E_t^{(v)} + \tau^{(v)}\hat{E}_i^{(v)} \right\|_2^2}{\left\| E_t^{(v)} \right\|_2^2} + \sum_{v=1}^{T} \frac{\left\| \chi\mathcal{A}_i\left[W^{(v)}\right] + \chi\tau^{(v)}\hat{E}_i^{(v)} - W^{(v)} \right\|_2^2}{\left\| \chi\hat{E}_i^{(v)} \right\|_2^2} \quad (4)$$

where the scattered field is split as $E_s = E_t - \tau\hat{E}_i$.

As it can be seen, the normalization herein considered for the first addendum is not the same as that of equation (3); in fact, the total field is considered instead of the scattered field because it represents the actual data of the problem.

The solution of the designing ISP problem can still be solved by minimizing the cost function (4) and by adopting the procedure developed in [41].

A simple modification of the proposed synthesis tool (see below) concerns the possible addition of penalty terms to the cost function to enforce some desired behaviors on the profile. In fact, besides the total field specifications, one could require some desired properties on the contrast function. Notably, the additive penalty terms enforce the desired behavior on χ, and the original term $\phi(W,\chi,\tau)$ penalizes the violation of the data and physical model mismatch [41],[43],[44]. In summary, the final optimization problem reads:

$$\min_{W,\chi,\tau} \phi' = \min_{W,\chi,\tau} \left(\phi + k_p\phi_p\right) \quad (5)$$

where k_p is a positive weighting coefficient of the occurring penalty term at hand. If k_p is sufficiently large, then the minimization is enforced to evolve inside or close to the set implicitly defined from the relevant constraint. More details on the choice of k_p are given in the numerical section.

A first possible requirement on χ (which is of interest in the following) could be enforcing a circular symmetry. In this case, the additive penalty term can be expressed as:

$$\phi_p = \phi_s = \left\| \frac{\partial\chi}{\partial\theta} \right\|_2^2 \quad (6)$$

because the minimization of ϕ_s prevents angular variations of the contrast function around the center of the coordinate system.

Similarly, the penalty term:

$$\phi_p = \phi_r = \left\| \frac{\partial\chi}{\partial r} \right\|_2^2 \quad (7)$$

prevents large radial variations of χ and hence provides a radially smooth contrast function.

A third useful requirement could be enforcing lossless and physical feasibility properties of the contrast function to possibly avoid the use of metamaterials. Clearly, this requirement is not strictly needed, but such a restriction can allow an easier manufacturing of the device. To this aim, the pertaining additional term can be formulated as follows:

$$\phi_p = \phi_f = \|\chi - f(\chi)\|_2^2 \quad (8)$$

where $f(\chi)$ is the projection of χ into the set of admissible functions (for example, the set of real and positive functions).

Finally, in the case of circularly symmetric profiles, an interesting chance to simplified manufacturing occurs in presence of a reduced number of materials when moving along the radial coordinate. Such a property is strictly related to the 'sparsity' concept underlying the Compressive Sensing (CS) framework [45] (see reference [45] for more details on the CS theory and references [13],[44],[46]–[49] for sparsity promoting techniques that are of interest herein). One can prove that the minimization of the ℓ_1-norm of the radial derivative of χ both enforces a piecewise constant behavior on the contrast profile and promotes the minimal number of hops in the synthesized lens. In such a case, the arising penalty term reads [13],[44]:

$$\phi_p = \phi_{sp} = \left\| \frac{\partial\chi}{\partial r} \right\|_1 \quad (9)$$

where $\|\cdot\|_1$ denotes the ℓ_1-norm.

Note that the reformulation of the cost function (4) (as well as the addition of penalty terms) leads to modification of both the gradient of the functional and of the coefficients in the line minimization step. For the sake of brevity, we do not provide the new expressions because they can be easily calculated following the procedure in [41] for the functional and [43],[44] for the penalty terms.

IV. Graded Artificial Materials (GAMs) design tools

The practical realization of GRIN structures is not a trivial task because of the need to realize arbitrary refractive index gradients in a controlled manner. To overcome this drawback, an approach toward a manufacture simplification could be an a-posteriori discretization of the GRIN profile by means of several shells [13]. In this case, some optimization procedures can be developed to reduce the foreseen degradation of the performances [19]–[21].

In the last decades, a great amount of effort has been devoted to realizing GRIN devices by means of structures made by properly arranged cylindrical dielectric or metallic rods [23]–[26], because such structures allow control of the electromagnetic waves propagation.

In the following, 2D GAMs comprised of dielectric rods are considered, and their design by means of a gradient of the filling factor (GAM_F) is proposed. Two different approaches are introduced that take advantage of the introduced inverse scattering methodologies and pursue the synthesis of a GAM_F: one is a quite straightforward strategy that amounts to exploitation of homogenization procedures on the solution of the ISP via equation (5) (see Section IV.A); the other is a more sophisticated strategy based on an original representation of the contrast function, followed by the use of analytically based equivalences among different small scatterers (see Section IV.B). Note that this second proposed approach leads to the intermediate design of GAMs featuring a gradient of the refractive index (GAM_R), which can be intrinsically relevant.

To introduce and validate the proposed tools in a simple yet significant case, we consider in the following a circularly symmetric profile. Notably, such a choice allows steering the beam (without incurring into any performance deterioration) by accordingly moving the primary sources.

As far as the arrangement of the rods in the GAMs structure is concerned, by taking inspiration from [27] a six-fold rotational symmetry is considered (see Fig. 1). Accordingly, the rods positions on the xy plane (except for the central one) are given by:

$$x_{k,h} = dk\cos\left(\frac{2h\pi}{6k}\right) \qquad y_{k,h} = dk\sin\left(\frac{2h\pi}{6k}\right) \tag{10}$$

wherein $k = 1..,K-1$ is the radial index scanning the rings, $h = 1,\dots,6H_k$ is the angular index, K and H_k are the total number of the rings for the arrangement of the rods and the number of inclusions along the k-th ring, respectively, and $d = (R-a)/K$ is the periodicity of the adopted triangular unit cell reported in Fig. 1, with R being the radius of the structure and a the radius of the rods.

A. Case 1: a Maxwell-Garnett driven procedure

The Maxwell-Garnett (MG) effective medium theory [32] is widely used to define the effective permittivity of AM-based structures with rods embedded in a host medium. Therefore, if the arrangement of the rods is known and a polarization for the field is chosen, by applying the MG mixing formulas [50] to a GRIN profile, the local permittivity value is realized by means of a proper choice of the radii of the different rods, to obtain a GAM_F structure comprised of rods of the same material.

The strategy proposed in this subsection applies the above-described homogenization theory to the continuous GRIN profile obtained by solving the ISP by minimizing the functional (5) (wherein a symmetric behavior has been enforced by means of the penalty term ϕ_s in (6)). Note that, to the best of our knowledge, to date, the mixing formulas have only been applied to realize canonical lenses whose refractive index function can be determined analytically [8],[27]–[31]. Herein, the mixing formulas are instead exploited for the (generic) GRIN distribution arising from the minimization of (5).

In more detail, the mixing formulas are exploited as summarized in the following:

- resample the GRIN profile $\varepsilon_r(\boldsymbol{r_s})$ synthesized by means of the modified CSI over a grid of N_p pixels ($s = 1,\dots,N_p$) in a very dense grid, thus obtaining a new GRIN profile $\varepsilon_r(\boldsymbol{r_{\tilde{s}}})$, with $\tilde{s} = 1,\dots,\tilde{N}_p$ and $\tilde{N}_p \gg N_p$;
- set K and H_k in equation (10);
- $\forall\, k$-th ring, estimate the pertaining radius for each h-th rod by means of the following formula [27]:

$$a_{kh} = \sqrt{\frac{S}{\pi N}\frac{(\varepsilon_b - \varepsilon_{r_{kh}})(\varepsilon_b + \varepsilon_F)}{(\varepsilon_b + \varepsilon_{r_{kh}})(\varepsilon_b - \varepsilon_F)}} \tag{11}$$

wherein ε_F is the permittivity value of the dielectric material chosen for the rods making up the GAM_F, S is the area of the adopted unit cell of the GAMs structure and N is the number of rods in the unit cell. Finally,

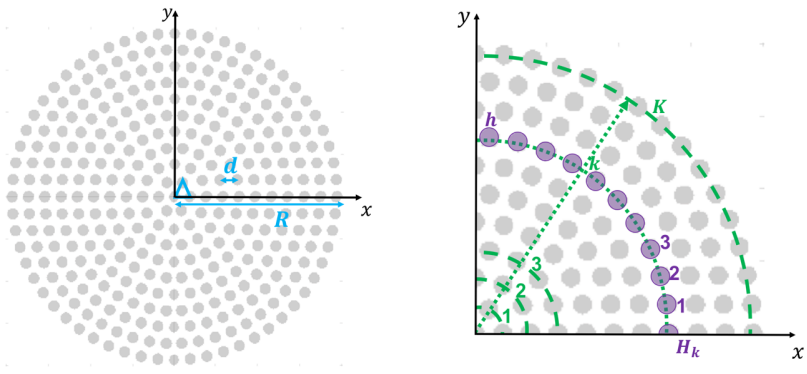

(a) (b)

Fig. 1. (a) AM-based structure with a six-fold rotational symmetry. The triangular unit cell is marked with solid blue lines. (b) Detail of the structure.

$\varepsilon_{r_{kh}} = \varepsilon_r(\boldsymbol{r_{kh}})$ is the permittivity value of the synthesized continuous GRIN profile evaluated in the position $\boldsymbol{r_{kh}}$, i.e., the center of the h-th rod belonging to the k-th ring (see Fig. 1).

Note that, because the GRIN profiles considered herein are circularly symmetric, the radius will be the same for all the rods belonging to the k-th ring, i.e., $a_{kh} \equiv a_k$.

B. Case 2: direct synthesis of GAMs

As an alternative to the GRIN-to-GAMs transition by means of homogenization procedures, in this subsection a completely different approach is introduced and discussed. In this approach, one first seeks a GAM_R structure as follows.

The unknown contrast function is expanded by means of a proper basis function that projects it into the 'space of rods', i.e.:

$$\chi(\boldsymbol{r}) = \sum_{k=1}^{K} \chi_k \sum_{h=1}^{H_k} \Pi\left(\frac{\boldsymbol{r} - \boldsymbol{r_{kh}}}{a_k}\right) \tag{12}$$

where χ_k is the contrast value associated with the k-th ring of rods, and each $\Pi\left(\frac{\boldsymbol{r}-\boldsymbol{r_{kh}}}{a_k}\right)$ function (which is associated with a single rod) is a circular window of radius a_k centered in $\boldsymbol{r_{kh}}$. As a consequence, the internal summation defines a composite window that is equal to one in each rod belonging to the k-th ring and is zero elsewhere.

By using representation (12) for the minimization of functional (5), the ultimate unknowns of the problem become the coefficients χ_k, which represent the contrast values of the rods belonging to the k-th ring.

Although this result is of intrinsic interest, a more interesting design solution is to determine GAM_F devices, in which the radii (in each ring) are instead the actual degrees of freedom of the problem. However, the direct search for the radii is a very difficult task because of the indirect manner the unknowns a_k enter into the ISP, thus increasing the non-linearity of the problem. A potential solution could be the joint exploitation of inverse scattering procedures and topology optimization techniques [51].

Very interestingly, by using classical analytical tools, one can exploit the (partial) result obtained by using (12) in the minimization of (5), i.e., the GAM_R structure, to synthesize in a simple fashion a GAM_F device. To be specific, smart determination of the radii can be pursued by taking advantage of the fact that the scattering behavior of each inclusion can be conveniently analyzed in terms of a so-called scattering matrix [52]. By adopting a cylindrical coordinate system placed in the center of each dielectric rod of radius a in the GAM_R structure, we can write an expansion in cylindrical harmonics for the incident ($\tilde{E}_i$), total ($\tilde{E}_t$) and scattered ($\tilde{E}_s$) field pertaining to each single inclusion [53]:

$$\tilde{E}_i(r,\theta) = \sum_{n=-\infty}^{+\infty} a_n J_n(\beta_0 r) e^{jn\theta} \tag{13}$$

$$\tilde{E}_t(r,\theta) = \sum_{n=-\infty}^{+\infty} b_n J_n(\beta r) e^{jn\theta} \tag{14}$$

$$\tilde{E}_s(r,\theta) = \sum_{n=-\infty}^{+\infty} c_n H_n^{(2)}(\beta_0 r) e^{jn\theta} \tag{15}$$

where a_n, b_n and c_n are the expansion's coefficients, J_n and $H_n^{(2)}$ are the n-th order Bessel function and Hankel function of second kind, respectively, and β is the wave number of the dielectric medium filling the cylinder.

According to the above cylindrical expansion, the "response" of each homogeneous cylindrical inclusion can be conveniently analyzed in terms of the scattering coefficients s_n=c_n/a_n. By enforcing the continuity conditions for the tangential components of the fields and by applying the recurrence formulas for the derivatives of the Bessel functions, one can finally obtain a compact expression for s_n, which reads as [54]:

$$s_n = \frac{(\beta a) J_{n-1}(\beta a) J_n(\beta_0 a) - (\beta_0 a) J_n(\beta a) J_{n-1}(\beta_0 a)}{(\beta_0 a) J_n(\beta a) H_{n-1}^{(2)}(\beta_0 a) - (\beta a) J_{n-1}(\beta a) H_n^{(2)}(\beta_0 a)} \tag{16}$$

Note that, besides the dependence on the radius a, s_n intrinsically depends on the contrast function χ through β_0 and β.

As long as the dielectric cylinder is sufficiently small with respect to the wavelength, one can easily verify by numerical or analytical tools that the term s_0 is much larger than all the others and the scattering phenomenon can be essentially

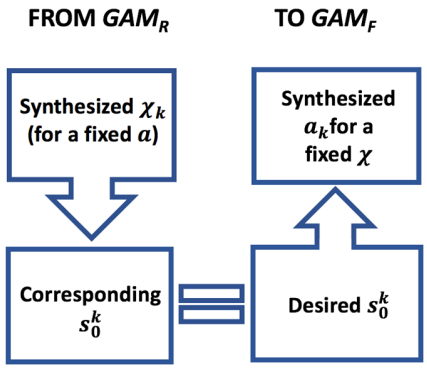

Fig. 2. Conceptual flow of the interchanging tool.

determined only from the $n = 0$ term. Thus, one can keep unaltered the behavior of s_0 (and, in a first instance, of the overall scattering phenomena) by performing an interchange between the local contrast value χ_k of the k-th rod and the radius a_k (see Fig. 2 for a conceptual sketch).

The guidelines of such an interchange are summarized in the following:

i. solve the inverse scattering problem by minimizing functional (5) using the representation (12) for the contrast (with a_k equal to a fixed value of a);
ii. for each k-th ring, namely, for each χ_k, evaluate $s_0(\chi_k, a)$ from equation (16) and denote it as $s_{0_{target}}^k$;
iii. for the selected material meant to realize the GAM_F (i.e., for the given value of χ), seek the radius most closely realizing the same scattering parameter, i.e.:

$$\min_{a_k} \left| s_0(\chi, a_k) - s_{0_{target}}^k \right|^2 \quad (17)$$

Note that the same type of derivation and procedure arguments can be eventually used in the case of metallic inclusions.

V. Synthesis of Lens Antennas Generating a Σ/Δ Reconfigurable (and Steerable) Pattern

The proposed inverse scattering-based design approach is quite general and hence applicable for different types of devices. In this paper, we assess the proposed technique with respect to the design of a lens antenna with radius $R = 3.1\lambda$ generating a Σ/Δ reconfigurable pattern [55], which is of interest for monopulse radar applications. Note that this is just one of the many possibilities that could be pursued using the proposed general approach.

In the literature, many methods are available for the synthesis of monopulse antennas; these methods typically rely on either arrays or reflectors [55]–[57]. With respect to common architectures, an interesting alternative could be represented by properly designed circularly symmetric dielectric lenses because they overcome beam degradation while avoiding a mechanical scanning of the entire structure.

The synthesis of the lens antenna is herein pursued by adopting the following three design steps:

i. *Definition of the far-field design constraints*: by exploiting the approach in [56] and considering the available degrees of freedom [58], two convenient 'optimal' far-field patterns (Σ and Δ) are synthesized that obey given mask constraints and goals.

ii. *Determination of the corresponding near-field to be pursued:* to avoid possible numerical drawbacks that could arise when considering far-fields, the observation domain Γ_o, which is supposed to be a circle (or a part of it), is positioned in the near-field region and a backpropagation (from the synthesized far-fields) is used to evaluate the target fields E_t on Γ_o. A rule of thumb is that of positioning Γ_o at least a wavelength from the overall radiating system (constituted by the primary sources and lens). Note that, in the case of directive patterns, the observation domain Γ_o does not need to completely enclose the lens, provided the field is sufficiently small in the neglected part.

iii. *Solution of the inverse scattering problem and design of the GAMs*: once the total field E_t on Γ_o is defined, the optimization problem involved in the modified CSI method is solved. Then, as the final goal of the approach is the design of a GAM_F device, the two alternative strategies described in Section IV can be applied.

Note step (i) leads to 'optimal' patterns that can be radiated by a continuous source with given dimensions. Starting from these patterns, the ISP should provide the dielectric distribution able to radiate the 'optimal' fields. However, there is no guarantee that a (physically feasible, non-active) permittivity profile such to realize those fields actually exist, so that some deteriorations from expectations are expected. Accordingly, it may be useful to adopt in step (i) design constraints more severe than the ones actually needed.

For the specific problem at hand, the outcome of point (i) is shown in Fig. 3. In particular, the 'optimal' Σ/Δ far-field patterns obeying the assigned mask constraints (dot-dashed lines), which are more severe than the ones finally required,

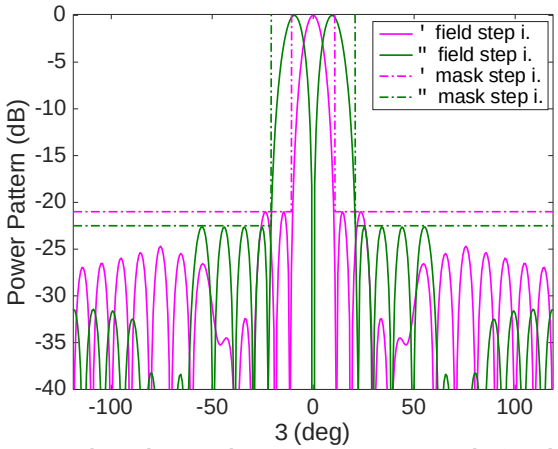

Fig. 3. Synthesized 'optimal' Σ (continuous magenta line) and Δ (continuous green line) patterns and relative mask constraints (dot-dashed lines).

are depicted. Starting from these synthesized fields, a back-propagation from the far-field coordinate $r_{o_{FF}} = 78\lambda$ to the near-field coordinate $r_o = 8\lambda$ was performed to determine the target fields E_t on Γ_o.

More details about points (i) and (ii) are given in the Appendix.

To solve the ISP, we considered $\hat{E}_i^{(v)}(r) = H_0^{(2)}(\beta_0 r)cos^4\vartheta$ as the primary source and $r = (r, \vartheta)$ as the coordinate of the generic point belonging to a reference system centered on the phase center of the feed. In particular, the design constraints imply that $T = 2$ primary incident fields must be used. By referring to Fig. 4, if the feed placed at $\theta_t = 0$ is active, the Σ-pattern is provided (magenta line in Fig. 3), and when the two feeds located at θ_t are simultaneously active and excited with an opposite phase, the corresponding total field will provide the Δ-pattern (green line in Fig. 3). The value of θ_t is set since from the step (i) as the first null of the Σ-pattern (see Appendix for details).

In all examples, numerical codes based on the method of the moments were exploited [59], and the region of interest Ω was discretized into $N_c \times N_c$ square cells. Note that, in the procedures described in Section IV, a very dense discretization was considered to correctly model the small circular windows involved in representation (12) as well as in the mixing formulas and the interchanging tool. To represent the reference field in a non-redundant fashion and to enforce an accurate fitting of the "measurements" data in equation (1), a number of sampling points as suggested in [58] was adopted. The fitting surface corresponds to the angular region of Γ_o ahead of the plane where the primary sources are located; thus, the complementary part was neglected because of the negligible impact on the far-field. Such a choice also allowed avoiding numerical issues related to the presence of the singularity in the source position.

In Table I, some other useful parameters involved in the numerical simulations are reported (see also Fig. 4).

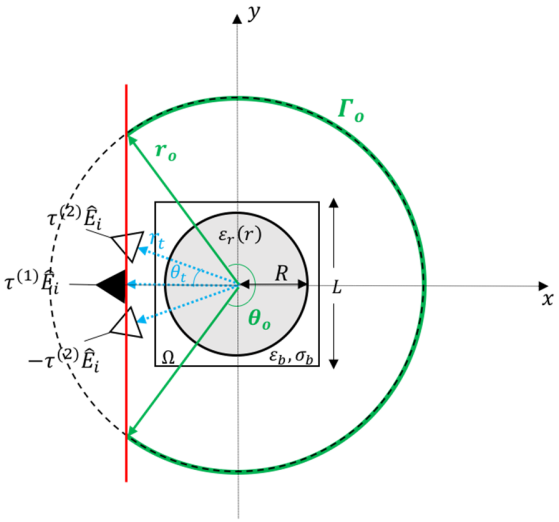

Fig. 4. The reference scenario for the numerical assessment. Two sets of excitations are depicted: if the "black triangle" antenna is active, then the Σ pattern is radiated; if the "white triangle" antennas are active and excited with an opposite phase, then the Δ pattern is radiated. The continuous red line is the plane of the Σ-feed, the green angular sector of Γ_o (dashed black line) represents the fitting surface.

For each example, the results were appraised in terms of beam-width (BW) and levels of the sidelobes (SLL) [60], and compared to the required specifications, that are $BW_\Sigma = 23°$ and $BW_\Delta = 46°$ $@-20dB$, $SLL_\Sigma = SLL_\Delta = -20dB$, respectively.

TABLE I
KEY PARAMETERS OF THE NUMERICAL EXPERIMENT

Parameter	Description	Value
L	Side of the region Ω	6.3λ
r_t	Distance of the primary source from the origin of the reference system	3.4λ
θ_t	Elevation angle of the primary sources	~10°
r_o	Radius of Γ_o	8λ
θ_o	Angular extension of the fitting surface	[-118.8°,118.8°]

A. *Lens design via Maxwell-Garnett driven procedure*

By following the strategy of Section IV-A, we first achieved the continuous GRIN lens shown in Fig. 5(a). In using the modified CSI method, we added the penalty terms ϕ_s and ϕ_f to the cost functional (4), to enforce circularly symmetric permittivity profiles and permittivity values real and larger than 1. Moreover, we enforced conductivity values $\sigma_r(\boldsymbol{r}) = 0$ to avoid power losses due to the propagation of the field inside the lens. Regarding the choice of the weighting parameters, we fixed k_s to be equal to the area of the pixel and k_f to be equal to the inverse of the area of the lens normalized to the square amplitude of the considered wavelength. Note that because we are dealing with a synthesis problem, the choice of the weighting parameters is not related to an a-priori rule. As such, the choice was supported by an extensively numerical analysis and the final k_p values were selected equal to the ones leading to the best radiative performances of the synthesized antenna.

To check the obtained performances, we evaluated the total field radiated by the synthesized continuous profile (Fig. 5(a)) when the designed GRIN lens is illuminated by primary sources with amplitude corresponding to the synthesized value of τ (see Table II). The resulting far field patterns are reported in Fig. 5 with the continuous blue lines. The total field radiated by the synthesized GRIN lens is found to be in good agreement with the far-field mask constraints (dot-dashed black lines).

Next, starting from the GRIN lens, we adopted the MG theory and the procedure described in Section IV-A by considering first $K = 11$ rings of rods comprised of SiO_2 material ($\varepsilon_r \equiv \varepsilon_F = 4.5$). Fig. 5(b) shows the obtained GAM_F, and the corresponding far-field patterns are reported in Fig. 5(d) and 5(f) with dashed red lines. As it can be seen, the total field radiated by the overall radiating system deviates from the initial field and the performances are deteriorated. On the other hand, when we increased the number of rings to $K = 14$, the GAM_F profile of Fig. 5(c) was obtained and better performances was achieved, see Fig. 5(e) and 5(g), and Table II for a quantitative comparison. Such a result is due to the limited capability of the homogenization procedure to deal with structures which are not dense in terms of rods and gradually variable in terms of permittivity profile of the synthesized continuous GRIN lens. Notably, by considering $\varepsilon_F = 8.9$, the MG-based approach completely failed (not shown for the sake of brevity).

To show the flexibility of the approach and the possibility to achieve better performances in case of gradually variable GRIN profile, we solved again the ISP by also considering the penalty term ϕ_r (meant to achieve a 'smooth' profile). In this case, the weighting parameter k_r was defined as a normalization factor with respect to the total number of discretizing cells and illuminating directions, and to the area of the single cell normalized to the wavelength. The thus obtained permittivity profile is depicted in Fig.6(a), while the pertaining radiated far-fields are shown with continuous blue lines in Fig. 6. Conversely, the dashed red lines in figures 6(d) and 6(f) are relative to the equivalent GAM_F lens reported in Fig.6(b), derived by the MG driven procedure for $K = 11$ and $\varepsilon_F = 4.5$. As it can be seen, also in this case the patterns are deteriorated. However, if a denser GAM_F lens is synthesized (see Fig. 6(c)) better performances are given as compared with the previous GAM_F solutions (see the dashed red lines in figures 6(e) and 6(g)). The synthetic parameters for the above example are summarized in Table III.

The achieved results allow to state that the proposed synthesis approach based on MG theory is capable in handling the same radiation patterns by also considering different permittivity distributions; however, the MG-based approach exhibits good performances as long as the GAM_F structure is filled by enough rods and the continuous GRIN profile exhibits smooth radial variations.

It is worth to stress that the requirements on the dielectric properties of the lens we are enforcing by means of penalty

terms in the cost function (especially the physical feasibility constraints (7)), in conjunction with the requirement of having a multi-purpose antenna, make the solution of the ISP very hard, so that unavoidable deteriorations of the performances are expected for increasing number of constraints.

with $\varepsilon_F = 4.5$ for the inclusions. The thus obtained GAM_F profile is shown in Fig. 7(b), and the corresponding fields in Figs. 7(c) and 7(d) (dashed red lines). As it can be observed, the resulting gradient of the filling factor allows to control the electromagnetic field path and to reach a good agreement with the initial specifications; see Table IV for a quantitative comparison.

Comparable performances were obtained for the synthesized lens with $K = 14$ and $a = \lambda/10$, whose

TABLE II
SYNTHETIC PARAMETERS FOR THE EXAMPLE IN FIG. 5

Profile	Synthesized $\tau^{(1)}$	Synthesized $\tau^{(2)}$	BW_Σ	$SLL_\Sigma\ (dB)$	BW_Δ	$SLL_\Delta\ (dB)$
GRIN lens	$3.5752 - j10.3729$	$-2.9171 + j9.4718$	25.5°	−22.3	44°	−18.95
MG GAM_F (K=11)			46°	−22.41	54°	−16.8
MG GAM_F (K=14)			30°	−19.52	55.5°	−18.46

TABLE III
SYNTHETIC PARAMETERS FOR THE EXAMPLE IN FIG. 6

Profile	Synthesized $\tau^{(1)}$	Synthesized $\tau^{(2)}$	BW_Σ	$SLL_\Sigma\ (dB)$	BW_Δ	$SLL_\Delta\ (dB)$
GRIN lens	$2.2673 - j10.7002$	$-1.8118 + j9.6339$	25.5°	−22	44°	−18.53
MG GAM_F (K=11)			46°	−22	55.5°	−16.9
MG GAM_F (K=14)			32°	−19.18	56°	−18.28

TABLE IV
SYNTHETIC PARAMETERS FOR THE EXAMPLE IN FIG. 7

Profile	Synthesized $\tau^{(1)}$	Synthesized $\tau^{(2)}$	BW_Σ	$SLL_\Sigma\ (dB)$	BW_Δ	$SLL_\Delta\ (dB)$
GAM_R lens	$-10.8198 + j2.6794$	$9.2811 + j2.9552$	22.6°	−25.67	46°	−18.9
GAM_F			24°	−21.84	48°	−16.75

TABLE V
SYNTHETIC PARAMETERS FOR THE EXAMPLE IN FIG. 8

Profile	Synthesized $\tau^{(1)}$	Synthesized $\tau^{(2)}$	BW_Σ	$SLL_\Sigma\ (dB)$	BW_Δ	$SLL_\Delta\ (dB)$
GAM_R lens	$-9.0933 - j4.6368$	$7.8344 + j4.4374$	23°	−25.38	42°	−18.71
GAM_F			24.6°	−23.24	48°	−17.7
GAM_F + losses			24.6°	−23.2	48°	−17.6

TABLE VI
SYNTHETIC PARAMETERS FOR THE EXAMPLE IN FIG. 9

Profile	Synthesized $\tau^{(1)}$	Synthesized $\tau^{(2)}$	BW_Σ	$SLL_\Sigma\ (dB)$	BW_Δ	$SLL_\Delta\ (dB)$
GAM_R lens	$-8.8183 - j5.3797$	$7.5927 + j5.0445$	23°	−26.9	45°	−17.9
GAM_F			23°	−26.2	46°	−18.22

B. Lens design via the "direct" procedure

To test the strategy introduced in Section IV-B, we first solved the modified CSI by considering in the expansion (12) $K = 11$ and $a = \lambda/8$ as well as the same arrangement of rods of the previous example. Moreover, in this case, the penalty term ϕ_f was added to the functional to consider simple materials. Fig. 7(a) shows the permittivity profile of the thus obtained GAM_R-based lens. By using the synthesized value of τ (see Table IV), the corresponding Σ and Δ far field patterns depicted in Figs. 7(c) and 7(d) (continuous blue lines) were achieved. As it can be seen, the new strategy that allows to directly synthesize the GAM_R structure works well, since the far-field patterns are in good agreements with the mask constraints.

Finally, we applied the analytic interchange procedure summarized in Fig. 2, by still considering a dielectric material pertaining profiles and far-fields are shown in Fig. 8, while the corresponding synthetic parameters are summarized in Table V. For this last case, we also tested the robustness of the proposed approach and the interchanging procedure by means of (17) in case of lossy inclusions; in particular, we considered $tan\delta = 0.001$ for SiO_2 at microwaves [61]. The corresponding patterns are depicted with dotted green lines in Fig. 8(c) and 8(d), from which it is possible to note that the performances keep almost unchanged with respect to the lossless case (see also Table V).

As expected, the larger the radius of the single inclusion (i.e., $a = \lambda/8$), the larger the mismatch between the radiated patterns from the GAM_R and the corresponding GAM_F antenna, due to higher approximation error in considering just the term $n = 0$ in (16). To corroborate all the above, we ran the design procedure with $K = 21$ and $a = \lambda/15$; by comparing the continuous blue line and the dashed red line in

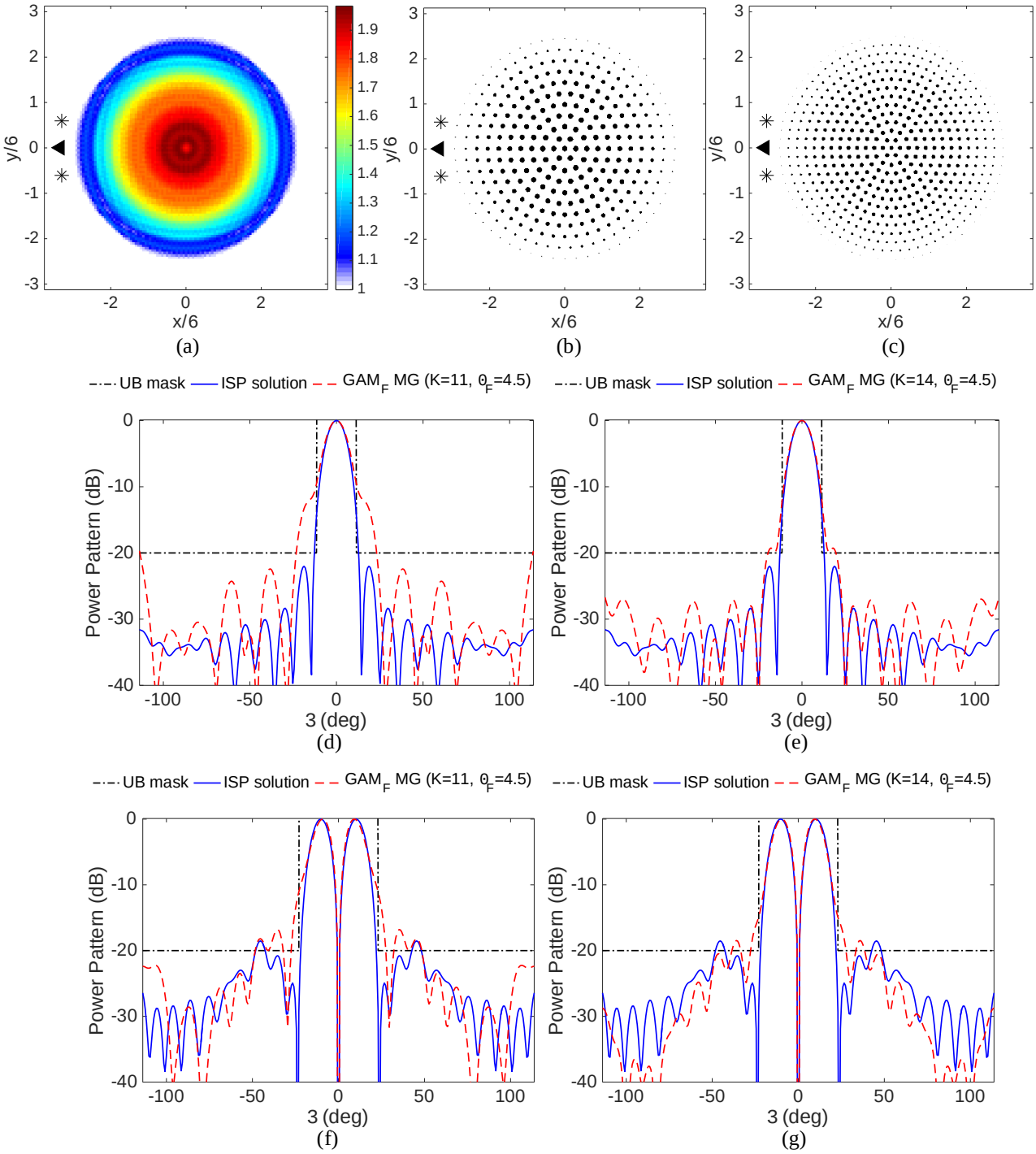

Fig. 5. Real part of the permittivity profile of the (a) GRIN lens as ISP solution when penalty terms ϕ_s and ϕ_f are exploited (k_s = 0.004, k_f = 0.0342, N_c = 99); equivalent GAM_F lens by MG (ε_F = 4.5, N_c = 1814) for (b) K = 11 and (c) K = 14. The black markers represent the location of the primary sources. Far field (d) Σ and (f) Δ power patterns radiated by profile-(a) (continuous blue lines) and profile-(b) (dashed red lines). (e)-(g) the same as (d)-(f) but relative to profile-(a) (continuous blue lines) and profile-(c) (dashed red lines). The dot-dashed black lines represent the expected mask constraints.

Fig. 9(c) and 9(d), and also the corresponding synthetic parameters in Table VI, it is possible to note that the far-field patterns for GAM_R and GAM_F fit very well.

Therefore, in the interchanging procedure a key role is played by the dimension of the rods. As a rule of thumb, one can define the radius of each rod at most equal to $a = \lambda/10$, the period d in (10) about $\lambda/7$ and then derive the needed number of rings K.

Finally, other examples (not shown herein) have demonstrated that, differently from the homogenization based

approach, the filling factor of the GAM_F structure does not substantially affect the performances.

VI. Conclusions

A new innovative tool was proposed for the design of two-dimensional Graded index Artificial Materials (GAMs) devices, starting from the solution of an inverse scattering problem.

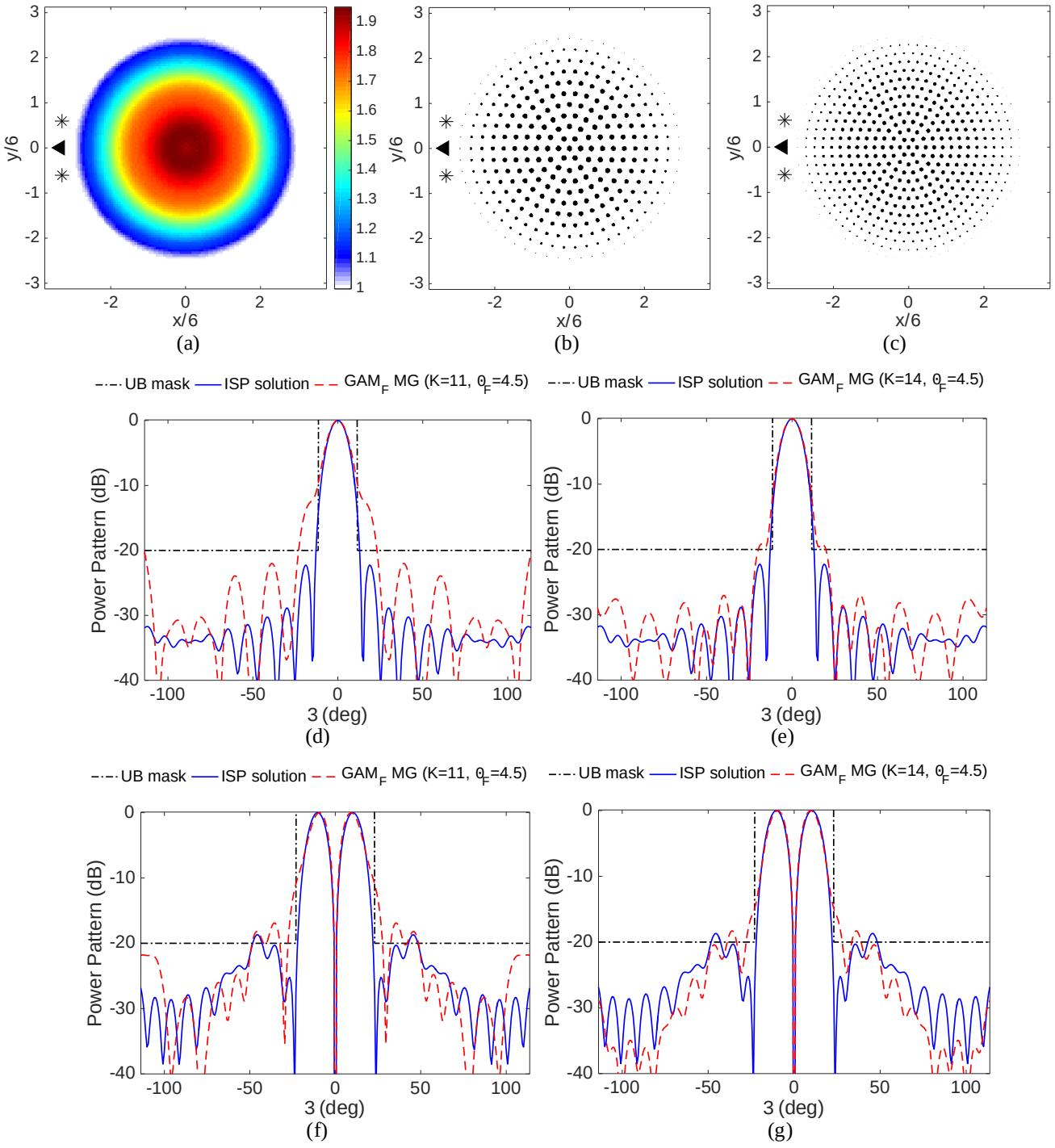

Fig.6. Real part of the permittivity profile of the (a) GRIN lens as ISP solution when penalty terms ϕ_s, ϕ_f and ϕ_r are exploited (k_s = 0.004, k_f = 0.0342, k_r = 10^{-6}, N_c = 99); equivalent GAM_F lens by MG (ε_F = 4.5, N_c = 1814) for (b) K = 11 and (c) K = 14. The black markers represent the location of the primary sources. Far field (d) Σ and (f) Δ power patterns radiated by profile-(a) (continuous blue lines) and profile-(b) (dashed red lines). (e)-(g) the same as (d)-(f) but relative to profile-(a) (continuous blue lines) and profile-(c) (dashed red lines). The dot-dashed black lines represent the expected mask constraints.

To this end, we first recast the Contrast Source Inversion method to: 1) provide a convenient setting of the amplitudes of the primary sources and 2) promote a desired behavior of the contrast function. Then, a first strategy to design GAMs with graded filling factor (GAM_F) was introduced by exploiting the widely used homogenization theories.

As a second opportunity, a novel expansion for the contrast function was proposed that allows for direct design of GAMs exploiting spatial variations of the refractive index among the different inclusions (GAM_R). These structures have two interesting aspects: 1) the refractive index of each inclusion can be eventually tuned (giving rise to very flexible devices)

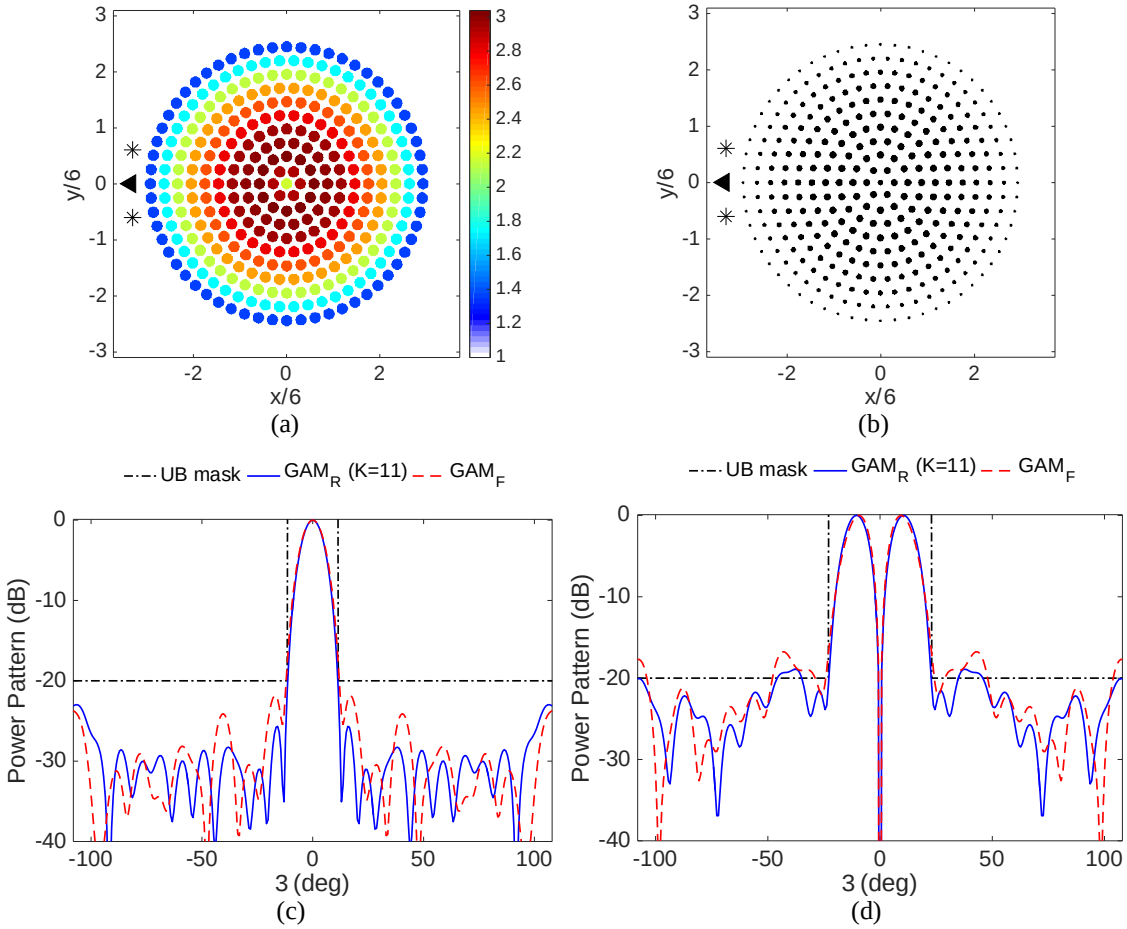

Fig.7. Real part of the permittivity profile of the (a) GAM_R lens (K = 11 and $a = \lambda/8$) as ISP solution when penalty term ϕ_f is exploited (k_f = 0.001, N_c = 626) and (b) equivalent GAM_F lens by fitting procedure (17) (ε_F = 4.5, N_c = 1822). The black markers represent the location of the primary sources. Far field (c) Σ and (d) Δ power patterns radiated by profile-(a) (continuous blue lines) and profile-(b) (dashed red lines). The dot-dashed black lines represent the expected mask constraints.

by using electro-optic or thermo-optic effects [62],[63] (or even the liquid crystal technology [38]) and 2) a simple analytical "interchanging" procedure applied on GAM_R structures allows to obtain an effective GAM_F solution.

The different tools were assessed through the synthesis of a monopulse antenna radiating a Σ/Δ reconfigurable pattern. Both proposed techniques are able to reach a good agreement with the desired specifications, although the second, and more original one, appeared to exhibit better performances. Note that, there is no guarantee that a (physically feasible, non-active) permittivity profile such to realize the 'optimal' patterns representing the design constraints exists, so that some deteriorations from expectations can be expected.

In all the presented examples, the overall synthesis procedure was found to take about 30 minutes on a computer equipped with an Intel Xeon E5-2687 W 3.10 GHz CPU and 256 GB RAM.

We stress that the proposed approaches and tools are not restricted to the realization of 'canonical' fields and that they can be applied to generic (physically feasible, see [58]) field specifications as well as using other unit cells for the definition of the GAMs structure.

According to the above encouraging results, which are also confirmed by preliminary 3D full-wave analysis of parallel plane based structures, future works will be devoted to the extension to 3-D geometries and other kinds of devices.

ACKNOWLEDGMENT

The authors would like to thank Professors F. Bilotti and V. Galdi for their valuable comments and suggestions.

APPENDIX

SYNTHESIS OF THE Σ/Δ PATTERNS

The aim of the field synthesis procedure is the determination of the target fields E_t on the observation points $\mathbf{r_o} \in \Gamma_o$ in the near-field region that fulfill the given mask constraints and specifications on the corresponding far-fields. To this end, let us consider an expansion of the Σ-field in circular harmonics for a 2D TM polarization:

$$E_\Sigma(\theta, r_{o_{FF}}) = \sum_{n=-\lceil\beta_0 R\rceil}^{\lceil\beta_0 R\rceil} \hat{\gamma}_n e^{jn\theta} \qquad \text{(A.1)}$$

where θ denotes the angular variable, R is the radius of the lens, $r_{o_{FF}}$ is the radius of a far-field observation circle, and:

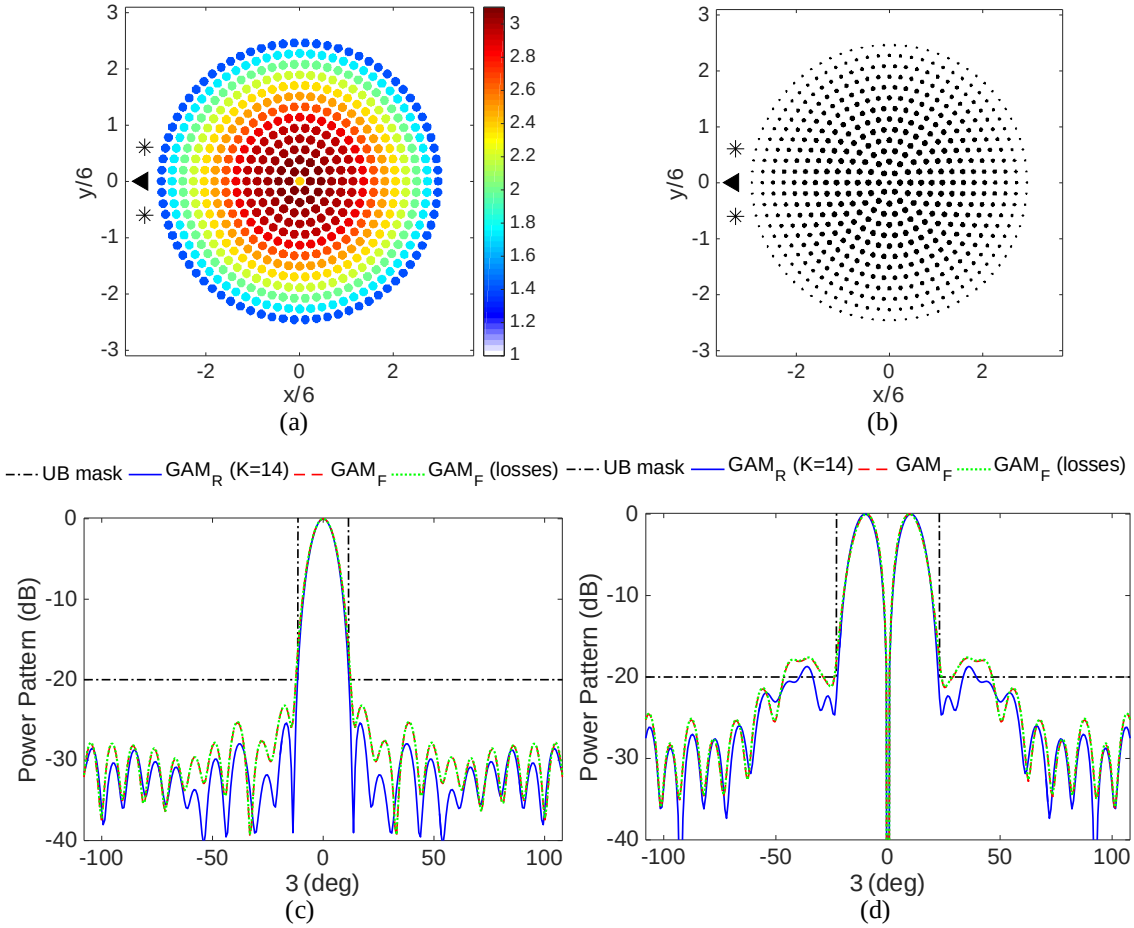

Fig.8. Real part of the permittivity profile of the (a) GAM_R lens (K = 14 and $a = \lambda/10$) as ISP solution when penalty term ϕ_f is exploited (k_f = 0.001, N_c = 626) and (b) equivalent GAM_F lens by fitting procedure (17) (ε_F = 4.5, N_c = 1822). The black markers represent the location of the primary sources. Far field (c) Σ and (d) Δ power patterns radiated by profile-(a) (continuous blue lines) and profile-(b) (dashed red lines). The dotted green lines are relative to profile-(c) in case of loss ($tan\delta$ = 0.001). The dot-dashed black lines represent the expected mask constraints.

$$\hat{\gamma}_n = \gamma_n H_n^{(2)}(\beta_0 r_{o_{FF}}) \tag{A.2}$$

are the expansion's coefficients. In (A.1), the summation is limited to $-\lceil\beta_0 R\rceil$, $\lceil\beta_0 R\rceil$ in accordance with the finite number of degrees of freedom associated with a source enclosed in a circle of radius R [58].

Thus, the Δ-field can be expressed as a linear combination of two Σ-fields shifted by θ_t and excited with an opposite phase:

$$\begin{aligned} E_\Delta(\theta, r_{o_{FF}}) &= E_\Sigma(\theta - \theta_t, r_{o_{FF}}) - E_\Sigma(\theta + \theta_t, r_{o_{FF}}) \\ &= \sum_{n=-\lceil\beta_0 R\rceil}^{\lceil\beta_0 R\rceil} \hat{\gamma}_n \left[e^{jn(\theta-\theta_t)} - e^{jn(\theta+\theta_t)}\right] \\ &= \sum_{n=-\lceil\beta_0 R\rceil}^{\lceil\beta_0 R\rceil} \hat{\gamma}_n \left[e^{-jn\theta_t} - e^{jn\theta_t}\right] e^{jn\theta} = \sum_{n=-\lceil\beta_0 R\rceil}^{\lceil\beta_0 R\rceil} \hat{\delta}_n e^{jn\theta} \end{aligned} \tag{A.3}$$

where $\hat{\delta}_n = -2j\sin(n\theta_t)\hat{\gamma}_n$. By so doing, only one of the $\hat{\gamma}_n$ and $\hat{\delta}_n$ sets of coefficients must be evaluated to perform the synthesis (the other one being related to it by a simple linear relationship).

Next, by noticing that expressions (A.1) and (A.3) resemble the expression of uniformly spaced array factors, one can follow the approaches respectively developed in the optimal "separate" synthesis of pencil [64] and difference [65] beams, as well as recent extensions to reconfigurable fields [56],[57]. By exploiting these results, the unknown coefficients can be finally determined by solving the following Convex Programming problem:

$$\min_{\hat{\gamma}_n} \left\{ -Re\left[\left.\frac{dE_\Delta(\theta)}{d\theta}\right|_{\theta=0}\right] \right\} \tag{A.4}$$

subject to:

$$\begin{cases} Re\left[\left.\dfrac{dE_\Delta(\theta)}{d\theta}\right|_{\theta=0}\right] \geq 0 & \text{(A.5a)} \\ E_\Delta(\theta = 0) = 0 & \text{(A.5b)} \\ |E_\Delta(\theta)|^2 \leq UB^\Delta(\theta) & \text{(A.5c)} \\ Re[E_\Sigma(\theta = 0)] = 1 & \text{(A.5d)} \\ Im[E_\Sigma(\theta = 0)] = 0 & \text{(A.5e)} \\ |E_\Sigma(\theta)|^2 \leq UB^\Sigma(\theta) & \text{(A.5f)} \end{cases}$$

where the objective function (A.4) and constraint (A.5a) allow for maximization of the amplitude of the (real) derivative of E_Δ in the target direction, constraints (A.5b), (A.5d) and

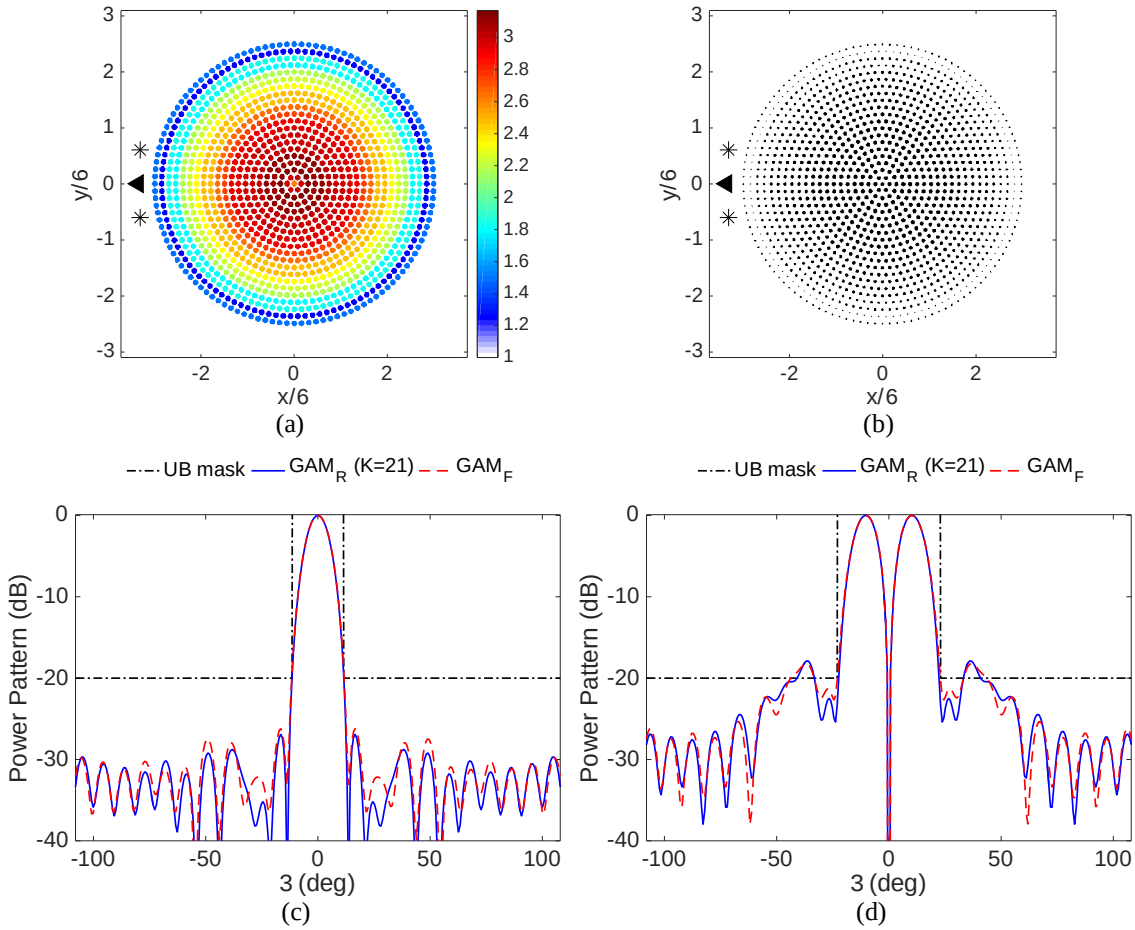

Fig.9. Real part of the permittivity profile of the (a) GAM_R lens (K = 21 and $a = \lambda/15$) as ISP solution when penalty term ϕ_f is exploited (k_f = 0.001, N_c = 626) and (b) equivalent GAM_F lens by fitting procedure (17) (ε_F = 4.5, N_c = 1822). The black markers represent the location of the primary sources. Far field (c) Σ and (d) Δ power patterns radiated by profile-(a) (continuous blue lines) and profile-(b) (dashed red lines). The dot-dashed black lines represent the expected mask constraints.

(A.5e) define the amplitude of the two fields in the target direction, and constraints (A.5c) and (A.5f) control the levels of the sidelobes of the two power patterns (UB^{Δ} and UB^{Σ} being suitable user-defined upper-bound masks).

It can be argued that an optimal choice of θ_t is the first null of the Σ-pattern. In fact, this choice allows a physical optimization of the Δ-pattern slope. After solving problem (A.4)-(A.5), the final expression of the two patterns on $\boldsymbol{r_o} \in \Gamma_o$ located in the near-field can be identified by a field backpropagation, i.e.:

$$E_{\Sigma}(\theta, r_o) = \sum_{n=-\lceil\beta_0 R\rceil}^{\lceil\beta_0 R\rceil} \gamma_n H_n^{(2)}(\beta_0 r_o) e^{jn\theta} \qquad (A.6)$$

$$E_{\Delta}(\theta, r_o) = E_{\Sigma}(\theta - \theta_t, r_o) + E_{\Sigma}(\theta + \theta_t, r_o) \qquad (A.7)$$

wherein, by virtue of (A.2), it is $\gamma_n = \hat{\gamma}_n / H_n^{(2)}(\beta_0 r_{o_{FF}})$.

REFERENCES

[1] S. P. Morgan, "General solution of the Luneberg lens problem," *J. Appl. Phys.*, vol. 29, no. 9, pp. 1358–1368, 1958.

[2] R. K. Luneburg and M. Herzberger, Mathematical theory of optics. University of California, 1964.

[3] Thomson, William, and Norman Macleod Ferrers., *The Cambridge and Dublin Mathematical Journal*, vol. 2. Macmillan, 1847.

[4] I. Aghanejad, H. Abiri, and A. Yahaghi, "Design of high-gain lens antenna by gradient-index metamaterials using transformation optics," *IEEE Trans. Antennas Propag.*, vol. 60, no. 9, pp. 4074–4081, 2012.

[5] Z. Duan, B.-I. Wu, J. A. Kong, F. Kong, and S. Xi, "Enhancement of radiation properties of a compact planar antenna using transformation media as substrates," *Prog. Electromagn. Res.*, vol. 83, pp. 375–384, 2008.

[6] W. X. Jiang, T. J. Cui, H. F. Ma, X. M. Yang, and Q. Cheng, "Layered high-gain lens antennas via discrete optical transformation," *Appl. Phys. Lett.*, vol. 93, no. 22, p. 221906, 2008.

[7] P.H. Tichit, S. N. Burokur, and A. de Lustrac, "Ultradirective antenna via transformation optics," *J. Appl. Phys.*, vol. 105, no. 10, p. 104912, 2009.

[8] Y. L. Loo, Y. Yang, N. Wang, Y. G. Ma, and C. K. Ong, "Broadband microwave Luneburg lens made of gradient index metamaterials," *J. Opt. Soc. Am. A*, vol. 29, no. 4, pp. 426–430, 2012.

[9] J. B. Pendry, D. Schurig, and D. R. Smith, "Controlling electromagnetic fields," *Sci.*, vol. 312, no. 5781, pp. 1780–1782, 2006.

[10] I. Gallina, G. Castaldi, and V. Galdi, "Transformation media for thin planar retrodirective reflectors," *IEEE Antennas Wireless Propag. Lett.*, vol. 7, pp. 603–605, 2008.

[11] M. Moccia, G. Castaldi, V. Galdi, A. Alu`, and N. Engheta, "Dispersion engineering via nonlocal transformation optics," *Optica*, vol. 3, no. 2, pp. 179–188, 2016.

[12] O. M. Bucci, I. Catapano, L. Crocco, and T. Isernia, "Synthesis of new variable dielectric profile antennas via inverse scattering techniques: a

feasibility study," *IEEE Trans. Antennas Propag.*, vol. 53, no. 4, pp. 1287–1297, 2005.
[13] T. Isernia, R. Palmeri, A. Morabito, and L. Di Donato, "Inverse scattering and compressive sensing as advanced em design tools," In: *Proceedings of the IEEE International Symposium on Antennas and Propagation & USNC/URSI National Radio Science Meeting*, pp. 433–434, 2017.
[14] L. Di Donato, L. Crocco, M. T. Bevacqua, and T. Isernia, "Quasi Invisibility via inverse scattering techniques," In: *Proceedings of the IEEE Conference on Antenna Measurements & Applications*, pp. 1–2, 2014.
[15] L. Di Donato, T. Isernia, G. Labate, and L. Matekovits, "Towards printable natural dielectric cloaks via inverse scattering techniques," *Sci. Rep.*, vol. 7, no. 1, p. 3680, 2017.
[16] M. Pastorino, Microwave imaging. John Wiley & Sons, vol. 208, 2010.
[17] D. Colton and R. Kress, Inverse acoustic and electromagnetic scatteringtheory, Springer Science & Business Media, vol. 93, 2012.
[18] T. Isernia, V. Pascazio, and R. Pierri, "On the local minima in a tomographic imaging technique," *IEEE Trans. Geosci. Remote Sens.*, vol. 39, no. 7, pp. 1596–1607, 2001.
[19] H. Mosallaei and Y. Rahmat-Samii, "Nonuniform Luneburg and two-shell lens antennas: radiation characteristics and design optimization," *IEEE Trans. Antennas Propag*., vol. 49, no. 1, pp. 60–69, 2001.
[20] B. Fuchs, L. Le Coq, O. Lafond, S. Rondineau, and M. Himdi, "Design optimization of multishell Luneburg lenses," *IEEE Trans. Antennas Propag.*, vol. 55, no. 2, pp. 283–289, 2007.
[21] B. Fuchs, O. Lafond, S. Rondineau, and M. Himdi, "Design and characterization of half Maxwell fish-eye lens antennas in millimeter waves," *IEEE Trans. Microw. Theory Techn*., vol. 54, no. 6, pp. 2292–2300, 2006.
[22] J. D. Joannopoulos, S. G. Johnson, J. N. Winn, and R. D. Meade, Photonic crystals: molding the flow of light. Princeton University, 2011.
[23] E. Centeno and D. Cassagne, "Graded photonic crystals," *Optics Lett.*, vol. 30, no. 17, pp. 2278–2280, 2005.
[24] F. Gaufillet and E´ . Akmansoy, "Graded photonic crystals for graded index lens," *Opt. Commun.*, vol. 285, no. 10, pp. 2638–2641, 2012.
[25] B. Vasic´, G. Isic´, R. Gajic´, and K. Hingerl, "Controlling electromagnetic fields with graded photonic crystals in metamaterial regime," *Opt. Express*, vol. 18, no. 19, pp. 20 321–20 333, 2010.
[26] O. Leonardi, G. Torrisi, L. Di Donato, A. Locatelli, L. Celona, C. De Angelis, and G. Sorbello, "Hollow-core electromagnetic band gap waveguide as DC-break for ion sources," In: *IEEE Progress In Electromagnetics Research Symposium-Spring*, pp. 1014-1017, 2017.
[27] X.-H. Sun, Y.-L. Wu, W. Liu, Y. Hao, and L.-D. Jiang, "Luneburg lens composed of sunflower-type graded photonic crystals," *Opt. Commun.*, vol. 315, pp. 367–373, 2014.
[28] Y.-Y. Zhao, Y.-L. Zhang, M.-L. Zheng, X.-Z. Dong, X.-M. Duan, and Z.-S. Zhao, "Anisotropic and omnidirectional focusing in Luneburg lens structure with gradient photonic crystals," *J. Opt.*, vol. 19, no. 1, p. 015605, 2016.
[29] F. Gaufillet and E. Akmansoy, "Graded photonic crystals for Luneburg lens," *IEEE Photon. J*., vol. 8, no. 1, pp. 1–11, 2016.
[30] W. Liu, X. Sun, M. Gao, and S. Wang, "Luneburg and flat lens based on graded photonic crystal," *Opt. Commun*., vol. 364, pp. 225–232, 2016.
[31] E. Falek and R. Shavit, "A parametric study on a 2D Luneburg's lens made of thin dielectric cylinders," In: *Proceeding of the IEEE International Symposium on Antennas and Propagation & USNC/URSI National Radio Science Meeting*, pp. 667–668, 2015.
[32] S. Datta, C. Chan, K. Ho, and C. M. Soukoulis, "Effective dielectric constant of periodic composite structures," *Phys. Rev. B*, vol. 48, no. 20, p. 14936, 1993.
[33] G. Peeler and D. Archer, "A two-dimensional microwave Luneberg lens," *IRE Trans. Antennas Propag.*, vol. 1, no. 1, pp. 12-23, 1953.
[34] F. Doucet, N.J. Fonseca, E. Girard, H. Legay, and R. Sauleau, "Analysis and design of a continuous parallel plate waveguide multiple beam lens antenna at Ku-band," In: *Proceedings of the 11th IEEE European Conference on Antennas and Propagation*, pp. 3631-3635, 2017.
[35] C. Pfeiffer and A. Grbic, "A printed, broadband Luneburg lens antenna," *IEEE Trans. Antennas Propag*., vol. 58, no. 9, pp. 3055–3059, 2010.
[36] M. Bosiljevac, M. Casaletti, F. Caminita, Z. Sipus, and S. Maci, "Non-uniform metasurface luneburg lens antenna design," *IEEE Trans. Antennas Propag*., vol. 60, no. 9, pp. 4065–4073, 2012.
[37] D. Gonza´lez-Ovejero, G. Minatti, G. Chattopadhyay, and S. Maci, "Multibeam by metasurface antennas," *IEEE Trans. Antennas Propag*., vol. 65, no. 6, pp. 2923–2930, 2017.
[38] S. Pavone, E. Martini, F. Caminita, M. Albani, and S. Maci, "Surface wave dispersion for a tunable grounded liquid crystal substrate without and with metasurface on top," *IEEE Trans. Antennas Propag.*, vol. 65, no.7, pp. 3540-3548, 2017.
[39] P. M. Van Den Berg and R. E. Kleinman, "A contrast source inversion method," *Inverse Probl*., vol. 13, no. 6, p. 1607, 1997.
[40] P. M. Van den Berg, A. Van Broekhoven, and A. Abubakar, "Extended contrast source inversion," *Inverse Probl*., vol. 15, no. 5, p. 1325, 1999.
[41] T. Isernia, V. Pascazio, and R. Pierri, "A nonlinear estimation method in tomographic imaging," *IEEE Trans. Geosci. Remote Sens*., vol. 35, no. 4, pp. 910–923, 1997.
[42] A. Abubakar and P. M. Van Den Berg, "Total variation as a multiplicative constraint for solving inverse problems," *IEEE Trans. Image Process.*, vol. 10, no. 9, pp. 1384–1392, 2001.
[43] L. Di Donato, M. T. Bevacqua, L. Crocco, and T. Isernia, "Inverse scattering via virtual experiments and contrast source regularization," *IEEE Trans. Antennas Propag*., vol. 63, no. 4, pp. 1669–1677, 2015.
[44] M. T. Bevacqua, L. Crocco, L. Di Donato, and T. Isernia, "Non-linear inverse scattering via sparsity regularized contrast source inversion," *IEEE Trans. Comput. Imaging*, vol. 3, no. 2, pp. 296–304, 2017.
[45] D. L. Donoho, "Compressed sensing," *IEEE Trans. Inf. Theory*, vol. 52, no. 4, pp. 1289–1306, 2006.
[46] D. W. Winters, B. D. Van Veen, and S. C. Hagness, "A sparsity regularization approach to the electromagnetic inverse scattering problem," *IEEE Trans. Antennas Propag*., vol. 58, no. 1, pp. 145–154, 2010.
[47] M. Ambrosanio and V. Pascazio, "A compressive-sensing-based approach for the detection and characterization of buried objects," *IEEE J. Sel. Topics Appl. Earth Observ. in Remote Sens.*, vol. 8, no. 7, pp. 3386–3395, 2015.
[48] P. Shah, U. K. Khankhoje, and M. Moghaddam, "Inverse scattering using a joint l1 − l2 norm-based regularization," *IEEE Trans. Antennas Propag*., vol. 64, no. 4, pp. 1373–1384, 2016.
[49] R. Palmeri, M. T. Bevacqua, L. Crocco, T. Isernia, and L. Di Donato, "Microwave imaging via distorted iterated virtual experiments," *IEEE Trans. Antennas Propag.*, vol. 65, no. 2, pp. 829–838, 2017.
[50] A. H. Sihvola, Electromagnetic mixing formulas and applications. Iet, no. 47, 1999.
[51] Bendsoe & Sigmund, Topology Optimization: Theory, Methods, and Applications, Springer, 2004.
[52] D. Felbacq, G. Tayeb, and D. Maystre, "Scattering by a random set of parallel cylinders," *JOSA A*, vol. 11, no. 9, pp. 2526-2538, 1994.
[53] D. S. Jones, "Acoustic and electromagnetic waves," Oxford/New York, Clarendon/Oxford University, p. 764, 1986.
[54] M. Abramowitz and I. A. Stegun, Handbook of mathematical functions: with formulas, graphs, and mathematical tables. Courier Corporation, 1964, vol. 55.
[55] R. S. Elliot, Antenna theory and design. John Wiley & Sons, 2006.
[56] A. F. Morabito and P. Rocca, "Optimal synthesis of sum and difference patterns with arbitrary sidelobes subject to common excitations constraints," *IEEE Antennas Wireless Propag. Lett*., vol. 9, pp. 623–626, 2010.
[57] P. Rocca and A. F. Morabito, "Optimal synthesis of reconfigurable planar arrays with simplified architectures for monopulse radar applications," *IEEE Trans. Antennas Propag*., vol. 63, no. 3, pp. 1048–1058, 2015.
[58] O. Bucci and T. Isernia, "Electromagnetic inverse scattering: Retrievable information and measurement strategies," *Radio Sci.*, vol. 32, no. 6, pp. 2123–2137, 1997.
[59] J. Richmond, "Scattering by a dielectric cylinder of arbitrary cross section shape," *IEEE Trans. Antennas Propag*., vol. 13, no. 3, pp. 334–341, 1965.
[60] C. A. Balanis, Antenna Theory. John Wiley & Sons, 1982.
[61] A. K. Mandal and S. Ranjan, "Microwave Absorption of Barium Borosilicate, Zinc Borate, Fe-Doped Alumino-Phosphate Glasses and Its Raw Materials," Technologies vol. 3, no. 2, pp. 111-125, 2015.
[62] U. Levy and R. Shamai, "Tunable optofluidic devices," *Microfluid Nanofluidics*, vol. 4, no. 1, pp. 97–105, 2008.
[63] C. Markos, K. Vlachos, and G. Kakarantzas, "Bending loss and thermo-optic effect of a hybrid pdms/silica photonic crystal fiber," *Opt. Express*, vol. 18, no. 23, pp. 24 344–24 351, 2010.

[64] T. Isernia, P. Di Iorio, and F. Soldovieri, "An effective approach for the optimal focusing of array fields subject to arbitrary upper bounds," *IEEE Trans. Antennas Propag.*, vol. 48, no. 12, pp. 1837–1847, 2000.

[65] O. Bucci, M. D'Urso, and T. Isernia, "Optimal synthesis of difference patterns subject to arbitrary sidelobe bounds by using arbitrary array antennas," In: *Proceedings of IEE Microwaves, Antennas and Propagation*, vol. 152, no. 3, pp. 129–137, 2005.